American Journal of Energy Engineering
2026, Vol. 14, No. 3, pp. 126–139
https://doi.org/10.11648/j.ajee.20261403.14

SciencePG
Science Publishing Group

Research Article

CFD Simulation via User-Defined Functions and Resizing of a Solar Dryer for Processing 25 kg of Pineapple

Alain Kossoun Tossa[1,*], **Said Ibrahim Adetayo Aballo**[2], **Orlane Naussica Lebama Aboughe**[3], **Odette Fokapu**[2]

[1]Laboratory of Energy and Applied Mechanics (LEMA), Abomey-Calavi Polytechnic School (EPAC), Cotonou, Benin
[2]Research and Development Department, Takaz-Eng, Cotonou, Benin
[3]Laboratory for Renewable Energy and Energy Efficiency, International Institute for Water and Environmental Engineering (2iE), Ouagadougou, Burkina Faso

Abstract

This article presents an optimization and numerical simulation (CFD) study of an indirect solar dryer designed for pineapple drying, aiming to reduce critical post-harvest losses in West Africa, particularly in Benin. Unlike many previous studies that are often limited to modeling an empty drying chamber, this work evaluates the system under real operational conditions by integrating an active load of 25 kg of pineapple. To achieve this, the authors utilize the ANSYS Fluent solver and develop three specific user-defined functions (UDF) to dynamically simulate coupled heat and mass transfers, thereby accurately representing the airflow resistance and active water evaporation within the product's porous matrix. Structurally, the system underwent several major geometric improvements, including resizing the solar collector to 5.54 m^2 to provide the 46.53×10^6 J required to extract 20.59 kg of water, and optimizing the spacing between trays to 250 mm. The results demonstrate that this new configuration effectively eliminates dead recirculation zones and ensures a homogeneous distribution of hot air. Quantitatively, the system maintains a highly uniform drying atmosphere, with temperature variations between the five trays limited to a narrow range of only 0.4 ℃ (52.9 ℃ to 53.3 ℃) and an inter-tray hygrometric gradient of less than 0.04%. While the model demonstrates high numerical robustness with a minimum orthogonal quality exceeding 0.1, the current lack of specific experimental validation for this resized configuration is acknowledged as a limitation, providing a foundation for future in situ correlation studies.

Keywords

Computational Fluid Dynamics (CFD), User-Defined Functions (UDF), Solar Drying, Ansys Fluent

1. Introduction

In West Africa, and more particularly in Benin, the agrifood sector suffers critical post-harvest losses ranging between 30% and 40% for perishable commodities [1]. These losses represent not only a major hindrance to the regional economy but also a direct threat to food security. In this context, pineapple is identified as a strategic new target product for industrial processing to reduce this waste [1]. Drying pineapple involves extracting a significant amount of water to reduce moisture

*Correspondence: Alain Kossoun Tossa (alain.tossa@uac.bj)

Received: 16 June 2026; **Accepted:** 30 June 2026; **Published:** 8 September 2026

content from 85% to 15%. This process requires precise thermal control to ensure product preservation and nutritional quality. This transition toward high-performance drying technologies is a necessity to ensure the nutritional quality of products and meet international food safety standards.

This study builds upon our previous work dedicated to the geometric optimization of an indirect solar dryer via numerical simulation (CFD) using fluid dynamics [2, 3]. While previous works focused on stabilizing thermal fluxes and eliminating dead zones within the empty drying chamber, the present work proposes to evaluate the system under real operational conditions by integrating an active load of 25 kg of pineapple. In the remainder of this article, first, a literature review examines critical performance factors and the limitations of current numerical simulations in the field of solar drying. The section dedicated to materials and methods then describes the geometric evolutions implemented for scaling up, as well as the multi-physics modeling strategy using user-defined functions (UDF) developed to simulate the interaction between air and pineapple. A specific chapter presents the optimized sizing of the solar collector required to satisfy the energy needs of a 25 kg load. Finally, the results and discussion section provides an in-depth analysis of the system's thermal, hydrodynamic, and kinetic performances, while validating the numerical robustness of the simulation before concluding on the prospects of this study.

2. State of the Art on Performance Factors and Numerical Modeling of Solar Dryers

2.1. Performance Factors of Solar Dryers

The overall performance of an indirect solar drying system is the result of a complex interaction between geometric, aerodynamic, and biological parameters. The scientific literature identifies several driving factors governing the efficiency of this process:

1) Areal loading density
2) Uniformity of air distribution
3) Management of solar intermittency
4) Air mass flow rate
5) Thermal potential of the flat-plate solar air collector

2.1.1. Areal Loading Density

Areal loading density constitutes a critical parameter governing airflow resistance and thermal efficiency within the drying chamber. According to the literature, density values for fresh products generally oscillate between 5 and 20 $kg \cdot m^{-2}$ of tray area [4], depending on product geometry and slice thickness (16 to 48 $kg \cdot m^{-2}$ for sliced and laminated products [5]). Singh et al. highlight the importance of load adequacy: an underloaded system can display a drying efficiency limited to only 4.1%, whereas an optimized load allows reaching an efficiency of 22.8% [6]. However, excessive density leads to compaction of the biological material, significantly increasing pressure drop and drastically reducing airflow [7]. This phenomenon can induce stagnation zones, local overheating, or incomplete drying of internal layers, thereby promoting microbial proliferation. To mitigate these risks, a physical compromise is often sought with fruit slice thicknesses between 4 and 8 mm [8], maximizing the exchange area while minimizing internal mass transfer resistance.

2.1.2. Uniformity of Air Distribution

Uniformity of air distribution is a determining parameter for ensuring homogeneous drying kinetics and guaranteeing the sanitary quality of the finished product. The scientific literature identifies inter-tray heterogeneity as one of the major obstacles to the industrialization of solar dryers [9]. This phenomenon is rigorously quantified by the uniformity index (Ui), which evaluates local velocity deviation from the mean, and the coefficient of variation (Cv), a critical indicator of mold risk on the slowest trays [9]. Computational fluid dynamics (CFD) simulation has demonstrated that stagnation zones often result from preferential fluid pathways bypassing the load ("bypass") or from flow blockage by the first trays. Several strategies can address these issues through geometric optimization. These include integrating distribution baffles [10], arranging trays in a zigzag pattern to enhance turbulent mixing [11], or using truncated pyramid outlets to improve moisture evacuation and air heating [12].

2.1.3. Management of Solar Intermittency

Managing solar intermittency poses a major challenge for the thermal stability of the process, as the common use of average daily irradiance values in analytical models masks critical temporal fluctuations [13]. Under real conditions, drying is an eminently unstable phenomenon where cloud passage, wind speed variations, and the evolution of the solar angle create transient boundary conditions.

To alleviate these instabilities, research is directed toward integrating thermal storage systems, whether sensible heat via pebble beds or latent heat using phase change materials (PCM) such as paraffin [14, 15]. These devices act as a thermal buffer capable of smoothing temperature gradients and extending the drying process for 3 to 4 hours after sunset [16]. Integrating these storage solutions not only stabilizes drying kinetics during cloudy periods but can also increase the overall system efficiency by more than 10% [14, 17] by ensuring the temperature is maintained between 1 and 8 ℃ above ambient during the night [18].

2.1.4. Air Mass Flow Rate

The air mass flow rate constitutes the fundamental coupling parameter between thermal energy collection in the collector and moisture extraction within the chamber. It acts as the primary operational lever to balance the temperature rise of the heat-transfer air and the overall thermal efficiency of the system.

The scientific literature highlights a critical thermodynamic trade-off: at low mass flow rates, air resides longer in the collector and reaches higher temperatures, but the device's efficiency drops because thermal losses to the outside increase with plate temperature. Conversely, higher flow rates improve collector efficiency through better cooling of the absorber, but the thermal elevation becomes insufficient to lower the relative humidity of the air, thereby restricting its water vapor transport capacity.

Reference works, notably those by Karim and Hawlader, suggest that a value of 0.035 $kg \cdot s^{-1}$ is optimal for drying most agricultural products [19, 20]. Maintaining the flow rate within a range of 0.01 to 0.05 kg/s is thus identified as the preferred strategy to maximize thermo-hydraulic efficiency while ensuring a constant drying potential [21].

2.1.5. Thermal Potential of the Solar Collector

The thermal potential of the flat-plate solar air collector acts as the thermodynamic engine of the system, dictating the air's ability to reach the optimal temperature range of 50 to 60 ℃ necessary for efficient and qualitative drying [22-24]. The scientific literature agrees that this potential is governed by a combination of optical properties and geometric configurations. Glass selection is crucial: a 4 mm thick glass is often identified as the ideal compromise, offering higher transmissivity than greater thicknesses while limiting convective losses [25].

Concerning the absorber, while copper performs best, aluminum constitutes the industrial standard for its conductivity-to-cost ratio [26], particularly when adopting a corrugated or V-corrugated geometry [27]. This shape increases thermal efficiency by 7 to 12% compared to flat plates by disrupting the laminar boundary layer and multiplying internal radiation reflections [27]. Finally, the thickness of the air gap is a major performance lever; studies demonstrate that a spacing of 50 to 55 mm allows collecting significantly more energy than a narrow or excessively wide channel, by balancing convective gains and thermal losses through the glazing [28]. Integrating these parameters into analytical models such as the Hottel-Whillier-Bliss model allows sizing the collection area to respond precisely to the energy demand linked to the product's latent heat of vaporization [29].

2.2. Sizing of the Solar Collector

The sizing of a flat-plate solar collector classically relies on a global energy balance relating the mass of water to be evaporated, the available solar irradiance, and the collector's efficiency. The fundamental equation for sizing the collection area Ac is written as [16, 30]:

$$Ac = \frac{Mw \cdot Lv}{(\eta c \cdot I \cdot ts)} \quad (1)$$

where Mw is the mass of water to be evaporated (kg), Lv is the latent heat of vaporization ($J \cdot kg^{-1}$), ηc is the collector efficiency, I is the average solar irradiance ($W \cdot m^{-2}$), and ts is the drying duration (s). This semi-empirical approach is used in nearly all published designs [16, 30, 31].

Several studies show that these global methods, although providing consistent sizing, exhibit major limitations. First, they assume a constant collector efficiency (typically 30-50% for an unglazed flat-plate collector, and 50-70% for a glazed collector) [17], whereas efficiency varies depending on airflow rate, inlet temperature, and instantaneous irradiance.

Second, irradiance I is generally taken as a daily average value, masking temporal variability that can lead to midday temperatures detrimental to product quality [32]. Thermal storage solutions using phase change materials (PCM) are proposed to mitigate these peaks and extend drying outside sunlight hours [32, 33].

Third, analytical sizing methods are not coupled to CFD simulations of the chamber. Collector design and internal flow simulation remain two sequential and decoupled stages in most studies: the flow rate and inlet temperature derived from the collector model are imposed as boundary conditions for the CFD simulation without iteration between the two models [12, 34]. Only a few recent works, such as that of Rani et al. [35] on a coupled mixed-mode dryer, attempt integrated collector-chamber-product modeling, but these approaches remain numerically expensive and difficult to transpose to real multi-tray configurations.

2.3. CFD Simulation

Computational fluid dynamics (CFD) simulation is currently an essential tool for analyzing the internal processes of solar dryers [36]. The drying chamber constitutes the main fluid domain of these simulations, but its geometric and physical representation varies considerably from one study to another [36].

In the vast majority of published works, the drying chamber is modeled as an empty enclosure, without explicit representation of the food product. The objective is then limited to predicting air velocity and temperature fields. Getahun et al. [37] report that most CFD studies on indirect solar dryers do not integrate product quality modeling. A recent review of CFD studies from 1984 to 2025 categorized dryers into cabinet, greenhouse, and tent types. It noted that simulations often model the chamber as a simple fluid domain, neglecting the water resistance of the product [36, 38].

When a product is present, it is usually represented by a passive thermal boundary condition, meaning a wall absorbing heat without returning water vapor to the fluid domain [37]. Demissie et al. [12] simulated a multi-tray indirect dryer in Ethiopia using ANSYS Fluent and predicted the velocity and temperature distribution on each tray, obtaining a maximum mean deviation of 4.3 ℃ between simulation and measurement. The trays are represented as porous surfaces permeable to the flow but without active evaporation. Amouiri et al. [39] simulated heat and mass transfers in an indirect dryer dedicated to medicinal plants, but the resolution of moisture diffusion within the product remains external to the CFD simulation.

The recent trend is to enrich the CFD domain with an equivalent hydraulic resistance representing the product bed (porous medium model) or by partial coupling with a distributed vaporization enthalpy balance [39]. These approaches improve the prediction of relative humidity at the chamber outlet but require knowledge of convective surface transfer coefficients, which are often derived from empirical correlations rather than calculated locally [35, 36].

The necessity of this active modeling approach is further supported by recent experimental investigations on similar high-moisture tropical fruit slices [40, 41]. Studies conducted at comparable air velocities (0.5-1.5 m/s) and temperatures (50-80 ℃) confirm that moisture removal occurs exclusively during the falling rate period, where internal diffusion is the governing mechanism [40, 42]. Quantitative analysis of these biological matrices reveals significant internal mass transfer resistance, providing a strong experimental basis for the use of User-Defined Functions to accurately capture the coupled heat and mass transfer dynamics within the product's porous matrix [41].

In conclusion of this literature review, recent research highlights the crucial importance of geometric optimization to ensure the aerodynamic and thermal efficiency of indirect solar dryers. It emerges that specific structural modifications, such as proper collector sizing, the adoption of a truncated pyramid top, or the precise adjustment of tray spacing, play a decisive role in reducing dead zones and homogenizing airflow. These design parameters now constitute a foundation of knowledge to maximize energy distribution within the drying chamber, thereby conditioning the overall performance of the installation.

Regarding numerical modeling, the state of the art also reveals inherent limitations in traditional computational fluid dynamics (CFD) approaches, which are mostly restricted to empty enclosures or representing food via simple passive thermal conditions. To capture the complexity of real drying dynamics, the literature converges on the need to integrate the physical behavior of products, notably through the porous media approach to accurately represent airflow resistance. Thus, modeling coupled heat and mass transfers, which accounts for the active evaporation of water contained in the product, has become a required methodological standard to evaluate a system under authentic operating conditions.

3. Materials and Methods

3.1. Reference Geometry and Implemented Modifications

The present work builds upon a baseline geometric configuration from our previous work (Figure 1), characterized by a 55 mm air gap, a 15 °inclination, and a corrugated absorber.

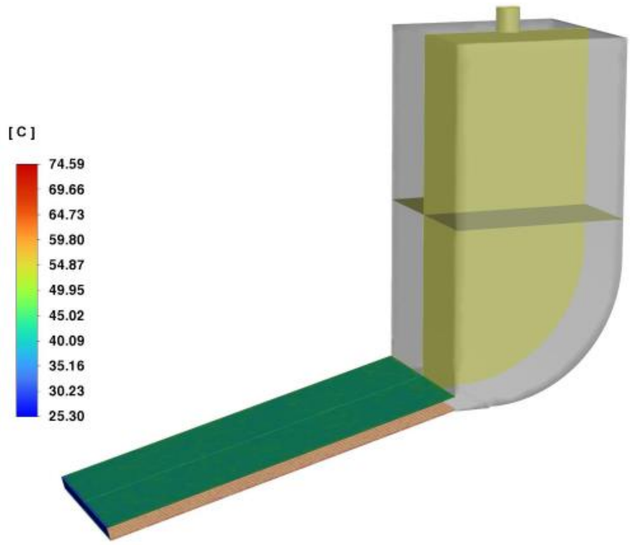

Figure 1. *Reference Geometry of the empty dryer.*

The transition from this empty optimized prototype to the resized configuration for an active load of 25 kg relies on a series of structural improvements dictated by recent research recommendations in solar drying.

1) Scaling up of the solar collector: Resizing the solar collector is a thermodynamic necessity to cover the energy requirement of 46.53 × 106 J required for the evaporation of 20.59 kg of water.
2) Funnel removal and direct axial flow: The removal of the lower funnel (present in the reference geometry) eliminates obstacles generating vortexes and dead zones. By making the flow purely axial toward the trays, the system minimizes local velocity gradients and ensures a more stable and direct flow toward the trays.
3) Truncated pyramid outlet: The upper part of the chamber now adopts a truncated pyramid geometry. This strategic design improves moisture evacuation while allowing additional heating of the air by diffuse radiation before its expulsion.
4) Chimney widening: The outlet duct has been increased to 100 mm in diameter, an optimal setting to balance the internal pressure required for air residence time and the efficient evacuation of saturating vapor.
5) Internal configuration (density < 5 kg/m^2 and 250 mm spacing): An optimized loading density (generally between 5 and 20 kg/m^2) is crucial to avoid excessive hydraulic resistance that would restrict the flow rate. The 250 mm spacing between the five trays exceeds the minimum recommendations (150-200 mm) to further reduce aerodynamic shading effects and guarantee inter-tray drying uniformity, a parameter often neglected but critical for industrial quality.

The biological load is modeled by pineapple slices with characteristic dimensions of 8.4 cm by 5.6 cm and a thickness of 1 cm, uniformly distributed across the different tray levels.

3.2. Meshing Strategy

Discretization of the numerical domain for the loaded system was achieved through a mixed meshing strategy using the ANSYS Meshing tool, balancing the geometric complexity of the resized chamber with the precision required at transfer interfaces. This high-resolution model includes a total of 2,788,034 cells and 557,122 nodes, a density selected to rigorously capture recirculation phenomena and thermo-hygrometric gradients. To model the aerodynamic interaction with the product without excessively complicating the topology, the five trays (named ananas_claie1 to ananas_claie5) were defined as porous zones. The porous media were initialized with a porosity of 0.7. Viscous and inertial resistance coefficients were set to 2.111e+08 m^{-2} and 500 m^{-1}, respectively, to accurately simulate the pressure drop caused by the pineapple slices. The validity of this discretization is attested by a minimum orthogonal quality of 0.105 (exceeding 0.30 for most tray areas), which remains well above the stability threshold of 0.01 recommended by numerical standards.

3.3. Physical Models and Boundary Conditions

The numerical simulation of this system is based on an integrated multi-physics approach under ANSYS Fluent, coupling fluid dynamics with heat and mass transfers. The turbulent flow regime is resolved via the SST k−ω model, selected for its accuracy in capturing gradients near walls and products, while radiative exchanges are treated by the Discrete Ordinate Model (DOM). Moisture transfer is modeled by the species transport model, treating water vapor as an active mass fraction within the fluid mixture. The originality of the modeling lies in the use of three user-defined functions (UDF): pineapple_vapor_source, pineapple_energy_latent, and pineapple_M_source, which respectively drive the source terms of mass, latent energy, and the evolution of the product's moisture content via a user-defined scalar (UDS-0).

The three user-defined functions (UDF) are defined as follows:

1) *pineapple_M_source:* This function defines the evolution of the local product moisture content, modeled as a user-defined scalar (UDS-0). It tracks the migration of internal moisture within the solid matrix over time.
2) *pineapple_vapor_source:* It calculates and injects the water vapor mass source term (Sw) into the fluid domain. This flux is proportional to the concentration gradient between the product surface and the ambient air, according to the formulation.

$$\dot{m}_{evap} = h_m . A\left(C_{surf} - C_{air}\right) \quad (2)$$

Where mevap (or Sw): Represents the water vapor mass flux, hm standardly designates the convective mass transfer coefficient involved in the proportionality of the flux, A represents the exchange surface area of the product with the air, Csurf corresponds to the water vapor concentration at the product surface, and Cair corresponds to the water vapor concentration in the ambient air.

3) pineapple_energy_latent: This UDF handles evaporative cooling by introducing an energy sink term into the heat equation. It accounts for the thermal energy consumed by the latent heat of vaporization during the phase transition of water from liquid to gas.

Regarding boundary conditions, the domain inlet is defined by a velocity of 0.5 m/s at a temperature of 25 ℃, while the outlet is maintained at zero-gauge pressure. The incident radiative flux follows a piecewise-linear irradiance profile varying from 340 to 717 W/m^2 (Figure 2), reproducing transient solar cycles to evaluate the dynamic response of the dryer.

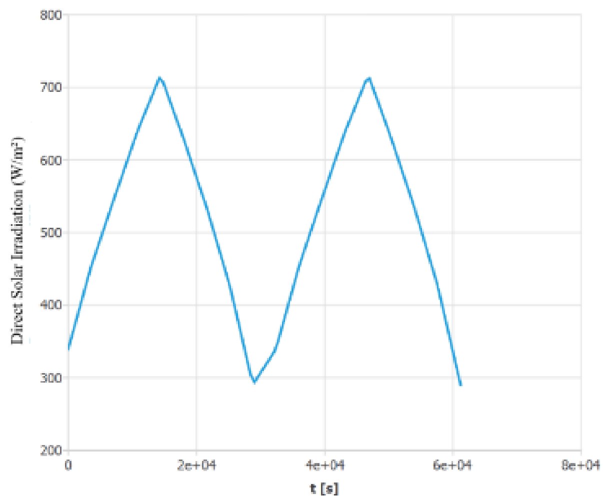

Figure 2. *Piecewise-linear Solar Irradiance Profile over Time.*

The biological load, modeled by a solid phase with a density of 995 kg/m^3 and a specific heat of 3,840 J/(kg K), is initialized with a dry basis moisture content of 5.67 kg water/kg dry_matter, corresponding to the initial 85% moisture content of fresh pineapple. These physical and numerical parameters ensure an accurate representation of the interaction between the heated air and the active porous matrix of the pineapple.

3.4. Modeling Pineapple Drying via UDF (Core Originality)

The core originality of this study lies in the implementation of an "active" multi-physics modeling of the biological product, moving beyond classical inert porous media approaches. To simulate the dynamic behavior of pineapple during drying, three user-defined functions (UDF) written in C language were developed and coupled to the ANSYS Fluent solver.

This approach relies on the integration of the specific thermophysical properties of pineapple, presented in Table 1:

Table 1. *Thermophysical properties of modeled pineapple.*

Property	Value
Density (ρ)	995 kg/m^3
Specific heat (Cp)	3 840 J/(kg K)
Thermal conductivity (λ)	0.51 W/(m K)

This strong coupling between species transport and custom scalars enables a dynamic feedback loop: the release of vapor locally humidifies and cools the air, which in turn modifies the drying potential for downstream trays.

3.5. Theoretical Sizing of the Collector

The theoretical sizing of the flat-plate solar air collector is based on a rigorous mass and energy conservation balance, aiming to align the thermal power supplied by solar radiation with the energy demand required for product water evaporation.

For a target load capacity of 25 kg of fresh pineapple (minitial) with an initial moisture content (Hinitial) of 85% (wet basis), the mass of dry matter (mdry) is first determined by the following equation:

$$m_{dry} = m_{initial} \times (1 - H_{initial}) \tag{3}$$

As the objective is to reach the final moisture content (Hfinal), the final mass of the product (mfinale) after processing is estimated by:

$$m_{final} = \frac{m_{dry}}{1 - H_{final}} \tag{4}$$

Consequently, the total mass of water to be extracted (mwater) for this load is:

$$m_{water} = m_{initial} - m_{final} \tag{5}$$

The total energy required for drying (Erequired) is obtained by multiplying this water mass by the latent heat of vaporization of water (Lv ≈ 2.26 × 10^6 J/kg):

$$E_{required} = m_{eau} \times Lv \tag{6}$$

The required collection area (Acollector) is then sized to satisfy this energy need under a design irradiance (I), a drying duration (t), and a collector efficiency (η):

$$A_{capteur} = \frac{E_{requise}}{I \times t \times \eta} \tag{7}$$

With I = 500 W/m^2, t = 6 h, η = 0.5.

By integrating a safety margin of 20% to account for potential solar radiation instabilities and thermal losses modeled by the Hottel-Whillier-Bliss equation

$$Q_u = A_c F_R[(\tau\alpha)_e I - U_L(T_{in} - T_a)] \tag{8}$$

$$A_{collector,secured} = A_{capteur} \times 1.20 \tag{9}$$

4. Results and Discussion

4.1. Results of Sizing, Meshing, and Initial Kinetics

Validation of the sizing and aerodynamic flow highlights the relevance of the modifications compared to the baseline prototype (which stabilized air temperature at 55.4 ℃ for an empty chamber). The transition to the resized configuration to support an active load, whose complete evolution of physical and structural parameters is recorded in Table 2, confirms the suitability of the technological choices. Scaling up the solar collector to 5.54 m^2 ensures the transfer of the theoretical energy input of 46.53 × 10^6 J, sufficient to cover the latent heat required for the evaporation of the 20.59 kg of water from the load. Aerodynamically, the new structural configuration, illustrated by Figure 3, removes the lower funnel in favor of a direct flow and adopts a truncated pyramid top. Combined with a chimney widened to 100 mm (optimizing internal pressure) and a 250 mm spacing between trays, this geometry eliminates recirculation zones (dead zones) and ensures a purely axial and homogeneous distribution of hot air under an active load of 25 kg.

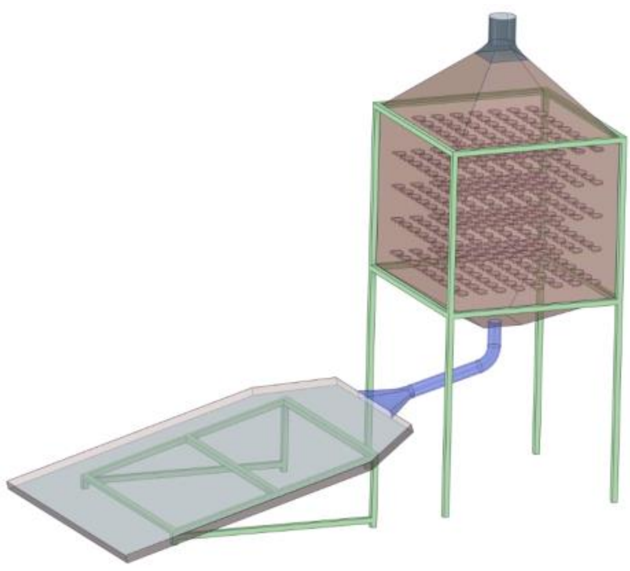

Figure 3. *3D View of the Optimized and Scaled-Up Solar Dryer.*

Table 2. *Evolution of geometric parameters between the initial prototype and the resized system.*

Component	InitialPrototype	Resized System
Collector area	~1.11 m^2	5.54 m^2
Collector dimensions	1.50 m x 0.74 m	2.52 m x 2.20 m
Chamber (L x w x h)	0.8 m x 0.8 m x 0.6 m	1.4 m x 1.3 m x 1.2 m
Tray spacing	-	250 mm

Regarding spatial discretization, independence tests resulted in an optimal configuration offering an excellent trade-off between computational cost and gradient capture accuracy. The topology and density of this discretization are highlighted in Figure 4 which shows the organization of meshes around the fruit trays. The numerical robustness of this model is directly validated by the geometric properties of the elements, detailed in Figure 5. The grid's minimum orthogonal quality exceeds 0.14, preventing numerical divergence. This ensures stable and accurate convergence for the transient solvers, especially at the complex interfaces between the fluid and the pineapple matrix.

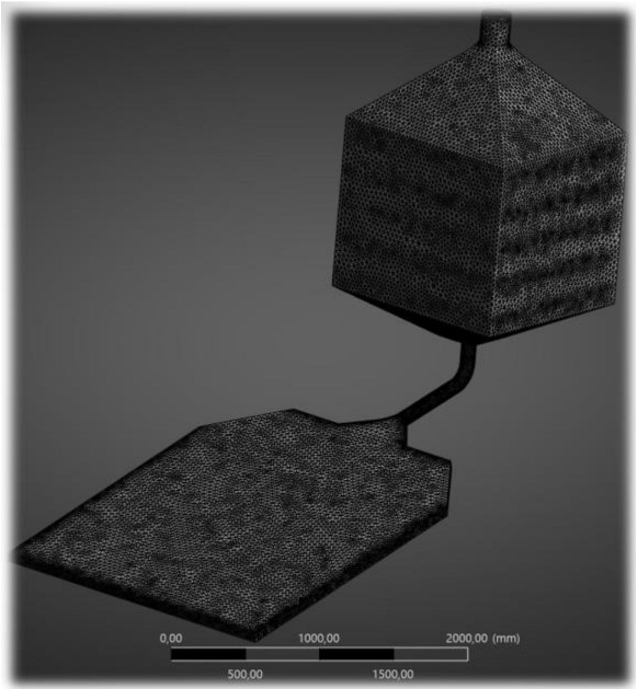

Figure 4. *Computational Mesh View of the Loaded Dryer Chamber.*

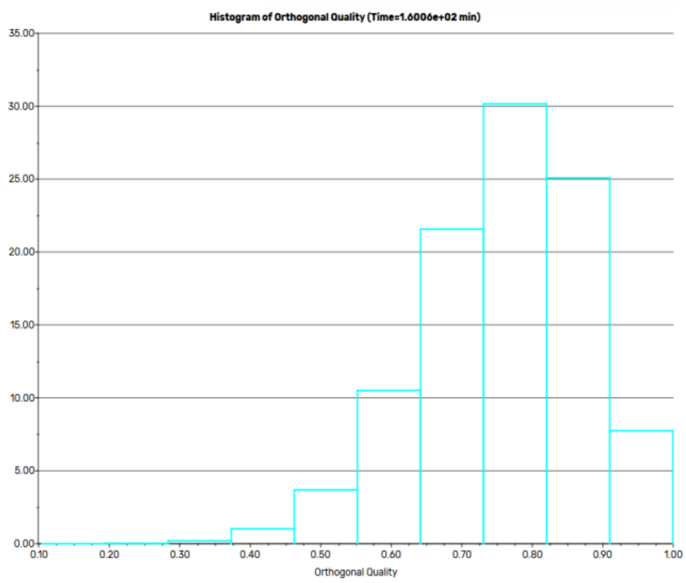

Figure 5. *Histogram of the Orthogonal Quality of Mesh Elements.*

System evaluation under a variable solar irradiance profile (oscillating between 340 and 717 W/m^2) confirms the proper functioning of the user-defined functions (UDF) developed to govern local mass transfers. During the first 160 minutes of simulation, the dry basis moisture content (M) of the entire load evolves steadily, dropping from its initial value of 5.67 kgwater/kgdry_matter (i.e., 85% wet basis moisture) to approximately 5.43 kgwater/kgdry_matter. Concurrently, active evaporation from the product locally alters the internal environment: the air surrounding the trays displays high relative humidity, ranging between 88.6% and 89.9%. These preliminary values validate the numerical coupling's ability to accurately capture the onset of drying and the migration of water vapor toward the evacuation zone.

4.2. Thermal Performance of the Loaded Chamber

In steady-state conditions (at 160 minutes of simulation), the system succeeds in maintaining a homogeneous drying atmosphere within the enclosure, with air temperatures across the five trays (C1 to C5) adjusting within a narrow range between 52.9 ℃ and 53.3 ℃. This performance perfectly aligns with literature recommendations prescribing a range of 50 to 60 ℃ to preserve the nutritional and organoleptic qualities of tropical fruits. The temperature of the corrugated absorber reaches 60.2 ℃, while the air at the chamber outlet is evacuated at 54.3 ℃.

However, a slight temperature drop is observed compared to the 55.4 ℃ obtained in the empty configuration of the initial prototype, which is explained by the latent heat consumption related to the evaporative cooling process induced by the active product. Figure 6 presents the overall thermal distribution from the collector to the drying chamber. Figure 7 presents a close-up view of the thermal contours on the surfaces of the pineapple slices to visualize surface uniformity.

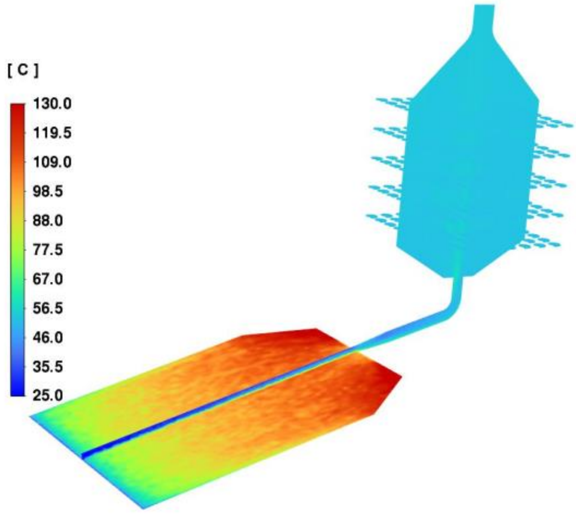

Figure 6. Global Thermal Distribution Profiles from the Collector to the Drying Cabinet.

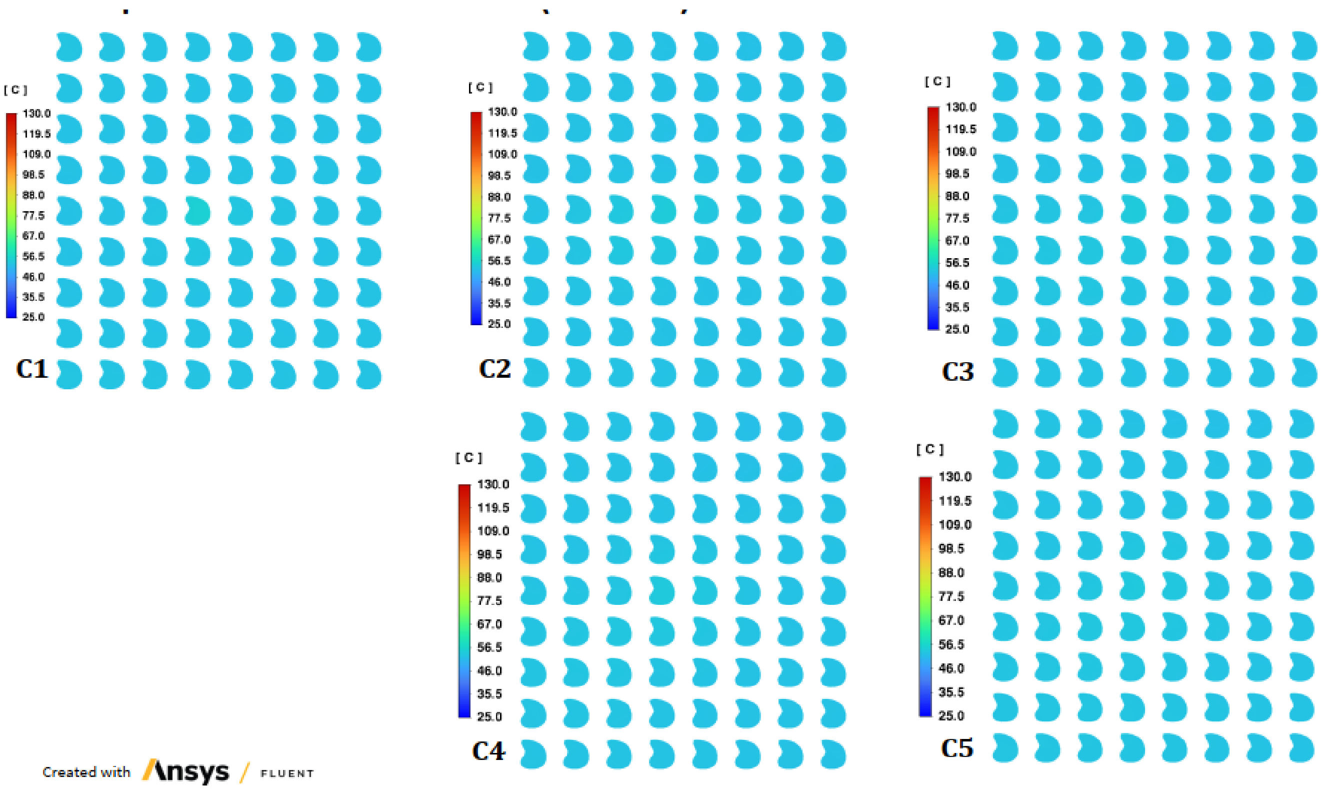

Figure 7. Close-up View of Temperature Contours on Pineapple Slice Surfaces Across Trays C1-C5.

Table 3 summarizes the temperature levels reached by the critical components of the loaded system:

Table 3. *Temperatures within the loaded dryer (t = 160 min).*

Component / Level	Simulated Temperature (℃)	Observation
Absorber (Aluminum)	60.20	Main heat source
Glazing (Glass)	34.43	External wall temperature
Air outlet (solar collector)	54.26	
Tray 1 (Inlet)	53.24	Hottest point in the load zone
Tray 2	53.05	-
Tray 3 (Middle)	52.98	-
Tray 4	52.91	-
Tray 5 (Outlet)	52.94	Minimum temperature in the load zone

4.3. Velocity Fields and Absence of Dead Zones

Hydrodynamic analysis of the loaded system reveals a particularly stable fluid behavior favorable to homogeneous drying. The simulated velocity profiles highlight a uniform airflow within the drying cabinet, marked by a total absence of significant dead zones. A notable acceleration phenomenon is observed at the connecting duct linking the collector to the chamber, where the air velocity undergoes a narrowing of streamlines to reach a peak of 11.63 m/s. This hot airflow then enters the expanded volume of the cabinet where it undergoes progressive deceleration, ensuring a regular distribution of velocity across all five trays. Figure 8 presents the three-dimensional velocity field from the collector outlet to the chimney, highlighting the acceleration to 11.63 m/s in the duct. Figure 9 visualizes the fluid's axial path and confirms the absence of turbulence or recirculation behind the trays.

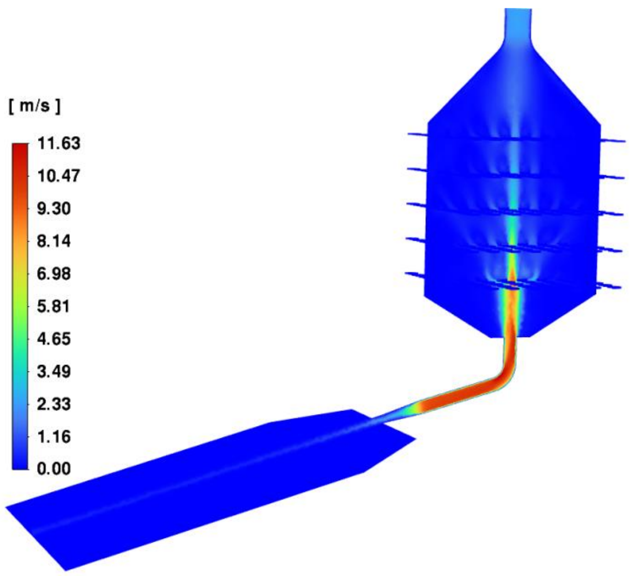

Figure 8. *Global Air Velocity Contour Fields.*

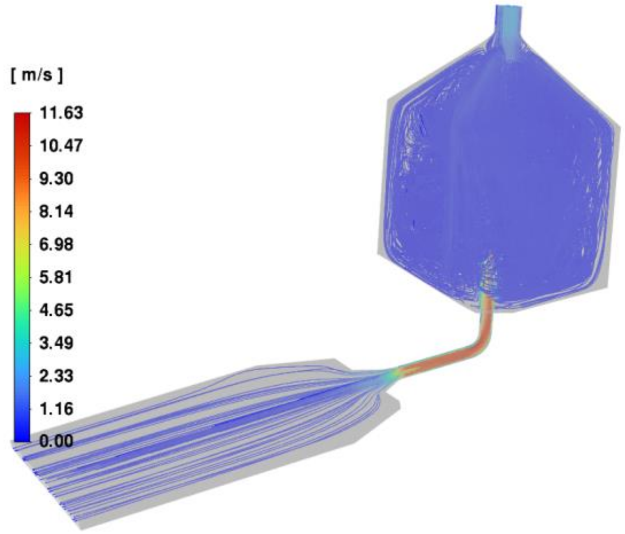

Figure 9. *Airflow Streamline Trajectories Through the Loaded Chamber.*

This aerodynamic behavior directly results from strategic geometric optimizations, notably the removal of the lower part of the cabinet (funnel) which, in the initial prototype, constituted a major obstacle generating vortexes and pockets of stagnant air. By making the flow more axial and stable, these modifications minimize local velocity gradients, ensuring that each pineapple slice benefits from a constant air renewal essential for water vapor evacuation. In comparison, whereas the original prototype suffered from massive stagnation zones hindering treatment homogeneity, the current configuration validates the robustness of the new design for a 25 kg load.

4.4. Pineapple Drying Kinetics

The analysis of pineapple drying kinetics, modeled via the multi-physics UDF-CFD coupling, allows tracking moisture migration within the 25 kg load in real time. Over the first 160 minutes of simulation, the dry basis moisture content (M) of the entire load evolves steadily, dropping from its initial value of 5.67 kgwater/kgdry_matter (corresponding to 85% wet basis moisture) to approximately 5.43 kgwater/kgdry_matter. This progressive reduction in moisture content confirms the proper functioning of the local mass source terms injected into the fluid domain. Concurrently, the atmosphere surrounding the trays exhibits high relative humidity, ranging between 88.6% and 89.9% at t = 160 min. These values, although higher than the drying air humidity in an empty configuration, are expected during the initial warm-up phase where the product is just beginning to release its water vapor.

An interesting result lies in the drying uniformity among the five trays. Final moisture content readings at 160 minutes show extremely small variations between tray 1 (inlet) and tray 5 (outlet), with values oscillating from 5.4299 for tray 1 to 5.4319 for tray 5. This absence of inter-tray hygrometric gradient (less than 0.04% deviation) validates the chamber resizing strategy and the absence of dead zones, ensuring that each product tier is processed under identical mass transfer conditions.

This kinetic stability, illustrated by the steady decrease of moisture content curves, demonstrates that the dryer resized to 5.54 m^2 provides sufficient evaporative power to maintain a constant drying potential despite progressive air saturation along the fluid path.

4.5. Validation of Collector Sizing

Simulations demonstrate that the initial collector of 1.11 m^2 (1.5 m x 0.74 m) was largely insufficient to provide the thermal power necessary to extract the 20.59 kg of water contained in the load.

Resizing to 5.54 m^2 (2.52 m x 2.20 m) allows precisely covering the total estimated energy need of 46.53 $\times 10^6$ Joules. Multi-physics simulation validates this choice by showing that, despite the evaporative cooling phenomenon which consumes a significant portion of the energy for latent heat, the system succeeds in maintaining a stable air temperature between 52.9 ℃ and 53.3 ℃ on the trays. This capability to stabilize the drying atmosphere within the optimal range (50-60 ℃) under a 25 kg load constitutes numerical proof of the sizing's validity.

4.6. Convergence Status and Numerical Validity

Analyzing the convergence status and numerical validity of the model constitutes a crucial step to ensure the reliability of multi-physics predictions within the loaded dryer. The increased complexity induced by introducing 25 kg of pineapple and active mass transfers required particular vigilance regarding mesh quality and residual behavior.

4.6.1. Mesh Quality and Discretization

The numerical domain, comprising 2,788,034 cells, was discretized to finely capture interactions at the air-product interface. Geometric validity is confirmed by a minimum orthogonal quality of 0.105 for the entire dryer. Although this value is lower than that of the empty mesh of the initial prototype, it remains well above the stability threshold of 0.01 recommended by numerical simulation standards. For critical tray zones, quality is even higher, oscillating between 0.28 and 0.42, which ensures accurate resolution of mass transfer gradients.

4.6.2. Analysis of Residual Convergence

Monitoring residuals at the end of the simulation (t = 160 min) reveals a differentiated behavior depending on the equations solved (Table 4):

Table 4. *Final convergence state of numerical residuals.*

Equation / Scalar	Final Residual	Convergence Criterion	Status
Continuity (Mass)	0.0832	0.001	Not Converged
Velocity (x, y, z)	~5e-06	0.001	Converged
Energy (Temperature)	6.37e-07	1e-06	Converged
k-omega model (Turbulence)	~2e-04	0.001	Converged
Species transport (h2o)	5.27e-09	0.001	Converged
Moisture content (uds-0)	3.93e-05	0.001	Converged
DO-intensity (Radiation)	5.80e-06	1e-06	Not Converged

Despite the strict non-convergence of continuity and radiation (DO-intensity) according to default criteria, model validity is maintained for the following reasons:

1) *Residual stabilization:* Continuity residuals stabilized at a constant level, which is common in complex simulations involving active porous media and UDF-CFD coupling.
2) *Radiation accuracy:* The DO-intensity residual (5.8e-06) remains slightly above the 1e-06 criterion, a performance deemed acceptable given the multiple reflections on the corrugated absorber and the semi-transparent nature of the glazing.
3) *Physical consistency:* The perfect convergence of energy, species transport, and user scalar (UDS-0) equations ensures that the thermal and hygrometric balances—the cores of the drying process—are resolved with high fidelity.

Overall, the stability of extracted physical parameters (tray temperatures, steady evolution of moisture content) confirms that the model is numerically robust and capable of predicting the system's real performance.

To provide a concise synthesis of the dryer's physical and numerical performance, Table 5 summarizes the key operating conditions and output metrics discussed in this study.

Table 5. *Compact summary of key operating conditions and dryer performance metrics.*

Category	Parameter / Metric	Value
	Inlet Air Velocity	0.5 m/s
	Solar Irradiance Range	340 - 717 W/m^2
Operating Conditions	Ambient Inlet Temperature	25 ℃
	Initial Pineapple Load	25 kg
	Initial Moisture Content	85% (wet basis)
Design Metrics	Optimized Collector Area	5.54 m^2
	Tray Spacing	250 mm
	Total Energy Supplied	46.53×10^6 J
	Total Water Extracted	20.59 kg
Performance Metrics	Average Tray Temperature	52.9 - 53.3 ℃
	Inter-tray Drying Uniformity	< 0.04% (hygrometric deviation)
	Mesh Orthogonal Quality	> 0.14 (minimum)

5. Conclusion

This study validated, through an advanced multi-physics modeling approach, the resizing and optimization of an indirect solar dryer intended for processing a target capacity of 25 kg of pineapple. The transition from a thermally insufficient initial prototype to a high-performance system relied on a rigorous methodology combining theoretical thermodynamic sizing and active numerical simulation. The originality of this work lies in the implementation of user-defined functions (UDF) enabling accurate simulation of the product's biological behavior and the evaporative cooling phenomenon, thus surpassing classical inert porous media modeling approaches. The numerical results demonstrate good inter-tray uniformity, with a temperature deviation of less than 1 ℃ among the five tiers and a total absence of dead zones thanks to the cabinet's aerodynamic optimizations. Scaling up validation confirms that the collection area must imperatively be increased to 5.54 m^2 to cover the energy needs of 46.53×10^6 J required for the extraction of 20.59 kg of water. The system thus dimensioned succeeds in stabilizing the drying atmosphere within the ideal range of 50 to 60 ℃, ensuring regular drying kinetics despite solar radiation variations. Despite the model's robustness, the partial convergence of the continuity equation and the current lack of specific experimental validation for this configuration constitute identified limitations. Looking forward, this work transforms an empirical design into a genuine predictive engineering tool, paving the way for a multi-objective optimization essential for sustainably reducing food waste in West Africa.

Abbreviations

CFD	Computational Fluid Dynamics
Cv	Coefficient of Variation
DO	Discrete Ordinates
DOM	Discrete Ordinates Model
PCM	Phase Change Material

SST	Shear Stress Transport
UDF	User-Defined Function
UDS	User-Defined Scalar
Ui	Uniformity Index

Acknowledgments

The authors gratefully acknowledge *Diasporeines Africa* for its valuable scientific and financial support, which contributed significantly to the successful completion of this research work.

Author Contributions

Alain Kossoun Tossa: Conceptualization, Methodology, Supervision

Said Ibrahim Adetayo Aballo: Formal Analysis, Writing – original draft

Orlane Naussica Lebama Aboughe: Software

Odette Fokapu: Writing – review & editing

Conflicts of Interest

The authors declare that they have no conflict of interest.

References

[1] World Bank, "*Benin Country Private Sector Diagnostic: Creating Markets in Benin – Mobilizing Private Investment to Spur Inclusive Growth.*" World Bank Group, Washington, D.C., 2023 " World Bank Group, Washington, D. C, 2023. [Online]. Available: https://documents.worldbank.org/en/publication/documents-reports/documentdetail/099923504172314185

[2] A. K. Tossa, S. I. A. Aballo, D. S. Takou, L. Djindi, G. C. Semassou, and O. Fokapu, "Development and Performance Evaluation of a Hybrid Solar Dryer with Latent Heat Storage and Dehumidification Systems," *Curr. J. Appl. Sci. Technol.*, vol. 44, no. 2, pp. 69-81, Feb. 2025, https://doi.org/10.9734/cjast/2025/v44i24485

[3] C. T. Nounangnonhou, K. A. Tossa, G. C. Semassou, and B. Nounagnon, "Design and Experimental Evaluation of a Fruits Hybrid-Solar Dryer," *Am. J. Energy Eng.*, 2023, https://doi.org/10.11648/j.ajee.20231104.12

[4] E. Menya and A. J. Komakech, "Investigating the effect of different loading densities on selected properties of dried coffee using a GHE dryer." [Online]. Available: https://cigrjournal.org/index.php/Ejounral/article/view/2270/1785

[5] S. Cansee, S. Saenkham, S. Hu, and T. Kanasri, "Effect of tray elevation and cassava load on solar drying performance, energy efficiency, and drying kinetics," *Results Eng.*, vol. 29, p. 109491, Mar. 2026, https://doi.org/10.1016/j.rineng.2026.109491

[6] S. Singh, P. P. Singh, and S. S. Dhaliwal, "Multi-shelf portable solar dryer," *Renew. Energy*, vol. 29, no. 5, pp. 753-765, Apr. 2004, https://doi.org/10.1016/j.renene.2003.09.010

[7] I. N. Simate, "Air Flow Model for Mixed-Mode and Indirect-Mode Natural Convection Solar Drying of Maize," *Energy Environ. Res.*, vol. 10, no. 2, p. 1, Sep. 2020, https://doi.org/10.5539/eer.v10n2p1

[8] A. E. Elwakeel *et al.*, "Modeling, environmental and economic analysis of drying of orange slice in an automatic indirect mixed mode solar dryer," *Sci. Rep.*, vol. 16, no. 1, p. 3898, Jan. 2026, https://doi.org/10.1038/s41598-025-29436-x

[9] H. H. Al-Kayiem and A. A. Gitan, "Flow uniformity assessment in a multi-chamber cabinet of a hybrid solar dryer," *Sol. Energy*, vol. 224, pp. 823-832, Aug. 2021, https://doi.org/10.1016/j.solener.2021.06.058

[10] H. Kidane, I. Farkas, and J. Buzás, "Enhancing the drying uniformity in solar drying systems: Computational and experimental study," *Int. J. Thermofluids*, vol. 29, p. 101408, Sep. 2025, https://doi.org/10.1016/j.ijft.2025.101408

[11] Tigabu Mekonnen Belay and Samson Mekbib Atnaw, "Design, CFD Simulation, Prototype, and Experimental Investigation of Indirect Active Solar Dryer for Banana," *Indian J. Prod. Therm. Eng.*, vol. 3, no. 5, pp. 1-18, Aug. 2023, https://doi.org/10.54105/ijpte.H9667.083523

[12] P. Demissie, M. Hayelom, A. Kassaye, A. Hailesilassie, M. Gebrehiwot, and M. Vanierschot, "Design, development and CFD modeling of indirect solar food dryer," *Energy Procedia*, vol. 158, pp. 1128-1134, Feb. 2019, https://doi.org/10.1016/j.egypro.2019.01.278

[13] S. Sami, A. Rahimi, and N. Etesami, "Dynamic Modeling and a Parametric Study of an Indirect Solar Cabinet Dryer," *Dry. Technol.*, vol. 29, no. 7, pp. 825-835, Jun. 2011, https://doi.org/10.1080/07373937.2010.545159

[14] H. E. Ferouali, A. Zoukit, I. Salhi, S. Doubabi, and N. Abdenouri, "Investigation of the efficiency of a solar dryer with thermal storage by rock salt and by pebble bed," *Int. J. Renew. Energy Technol.*, vol. 10, no. 4, p. 283, 2019, https://doi.org/10.1504/IJRET.2019.102845

[15] A. El Khadraoui, S. Bouadila, S. Kooli, A. Farhat, and A. Guizani, "Thermal behavior of indirect solar dryer: Nocturnal usage of solar air collector with PCM," *J. Clean. Prod.*, vol. 148, pp. 37-48, Apr. 2017, https://doi.org/10.1016/j.jclepro.2017.01.149

[16] E. L. Rulazi, J. Marwa, B. Kichonge, and T. Kivevele, "Development and Performance Evaluation of a Novel Solar Dryer Integrated with Thermal Energy Storage System for Drying of Agricultural Products," *ACS Omega*, vol. 8, no. 45, pp. 43304-43317, Nov. 2023, https://doi.org/10.1021/acsomega.3c07314

[17] A. Fudholi and K. Sopian, "A review of solar air flat plate collector for drying application," *Renew. Sustain. Energy Rev.*, vol. 102, pp. 333-345, Mar. 2019, https://doi.org/10.1016/j.rser.2018.12.032

[18] N. Meneceur, I. Bouaziz, K. Aliouat, K. Deghoum, and Y. Aoun, "Design and evaluation of an indirect solar dryer with a phase change material-integrated collector for thermal energy storage," *J. Stored Prod. Res.*, vol. 117, p. 103015, May 2026, https://doi.org/10.1016/j.jspr.2026.103015

[19] B. N. D. Pagukuman and M. K. Wan Ibrahim, "A review of the significance effect of external factors of the solar dyer design to dried foods product quality," *J. Eng. Des. Technol.*, vol. 20, no. 6, pp. 1765-1786, Dec. 2022, https://doi.org/10.1108/JEDT-01-2021-0033

[20] M. A. Karim and M. N. A. Hawlader, "Performance evaluation of a v-groove solar air collector for drying applications," *Appl. Therm. Eng.*, vol. 26, no. 1, pp. 121-130, Jan. 2006, https://doi.org/10.1016/j.applthermaleng.2005.03.017

[21] M. Y. Doshi, A. Jain, and K. N. Patil, "Performance Analysis of Solar Air Dryer for Multi Crop Drying Effect of Varying Air Mass Flow Rate," *SSRN Electron. J.*, 2017, https://doi.org/10.2139/ssrn.3101275

[22] T. O. Ajao *et al.*, "Comparative Study of the Drying Rate, Drying Kinetics and Sensory Evaluation of Mango Chips Using a Cabinet Tray Dryer and a Solar Dryer," *Turk. J. Agric. - Food Sci. Technol.*, vol. 13, no. s2, pp. 3518-3528, Nov. 2025, https://doi.org/10.24925/turjaf.v13is2.3518-3528.8070

[23] W. Wang, M. Li, R. H. E. Hassanien, Y. Wang, and L. Yang, "Thermal performance of indirect forced convection solar dryer and kinetics analysis of mango," *Appl. Therm. Eng.*, vol. 134, pp. 310-321, Apr. 2018, https://doi.org/10.1016/j.applthermaleng.2018.01.115

[24] L. F. Santis-Espinosa, B. Y. Perez-Sariñana, C. A. Guerrero-Fajardo, S. Saldaña-Trinidad, E. C. López-Vidaña, and S. Pathiyamattom-Joseph, "Drying Mango (Mangifera indica L.) with Solar Energy as a Pretreatment for Bioethanol Production," *BioResources*, vol. 10, no. 3, pp. 6044-6054, Aug. 2015, https://doi.org/10.15376/biores.10.3.6044-6054

[25] R. Bakari, R. J. A. Minja, and K. N. Njau, "Effect of Glass Thickness on Performance of Flat Plate Solar Collectors for Fruits Drying," *J. Energy*, vol. 2014, pp. 1-8, 2014, https://doi.org/10.1155/2014/247287

[26] Amrizal, Amrul, Ahmad Yonanda, and Zulfa, "Comparison Study of Solar Flat Plate Collector With Two Different Absorber Materials." 2017. [Online]. Available: https://www.researchgate.net/publication/341189167_Comparison_Study_of_Solar_Flat_Plate_Collector_With_Two_Different_Absorber_Materials

[27] A. E. Kabeel, A. Khalil, S. M. Shalaby, and M. E. Zayed, "Experimental investigation of thermal performance of flat and v-corrugated plate solar air heaters with and without PCM as thermal energy storage," *Energy Convers. Manag.*, vol. 113, pp. 264-272, Apr. 2016, https://doi.org/10.1016/j.enconman.2016.01.068

[28] N. M. Nahar and M. P. Gupta, "Studies on gap spacing between absorber and cover glazing in flat plate solar collectors," *Int. J. Energy Res.*, vol. 13, no. 6, pp. 727-732, 1989, https://doi.org/10.1002/er.4440130611

[29] H. Mzad and F. Bennour, "A simple graphical method for sizing flat-plate solar air heaters based on transversal and longitudinal aspect ratios," *Heat Transf.*, vol. 53, no. 8, pp. 4668-4694, Dec. 2024, https://doi.org/10.1002/htj.23153

[30] Md. S. Hossain *et al.*, "Design, fabrication, and performance evaluation of an indirect solar-powered vegetable dryer," *Sol. Energy Adv.*, vol. 5, p. 100096, 2025, https://doi.org/10.1016/j.seja.2025.100096

[31] O. A. Babar, A. Tarafdar, S. Malakar, V. K. Arora, and P. K. Nema, "Design and performance evaluation of a passive flat plate collector solar dryer for agricultural products," *J. Food Process Eng.*, vol. 43, no. 10, p. e13484, Oct. 2020, https://doi.org/10.1111/jfpe.13484

[32] T. B. Devi *et al.*, "Solar dryer using evacuated tube solar thermal collector with thermal storage," *Indian J. Agric. Sci.*, vol. 93, no. 2, pp. 233-236, Feb. 2023, https://doi.org/10.56093/ijas.v93i2.109915

[33] G. Xu and H. Liu, "Efficiency analysis of solar drying system integrated with flat-plate solar collector and thermal storage units," *Renew. Energy*, vol. 243, p. 122569, Apr. 2025, https://doi.org/10.1016/j.renene.2025.122569

[34] E. Castillo-Orozco, O. Garavitto, O. Saavedra, and D. Mantilla, "The Drying Kinetics and CFD Multidomain Model of Cocoa Bean Variety CCN51," *Foods*, vol. 12, no. 5, p. 1082, Mar. 2023, https://doi.org/10.3390/foods12051082

[35] P. Rani and P. P. Tripathy, "CFD coupled heat and mass transfer simulation of pineapple drying process using mixed-mode solar dryers integrated with flat plate and finned collector," *Renew. Energy*, vol. 217, p. 119210, Nov. 2023, https://doi.org/10.1016/j.renene.2023.119210

[36] H. Kidane, I. Farkas, and J. Buzás, "Modeling airflow dynamics in solar drying chambers: a comprehensive review of CFD applications," *Discov. Appl. Sci.*, vol. 7, no. 5, p. 444, May 2025, https://doi.org/10.1007/s42452-025-06894-6

[37] E. Getahun, M. A. Delele, N. Gabbiye, S. W. Fanta, P. Demissie, and M. Vanierschot, "Importance of integrated CFD and product quality modeling of solar dryers for fruits and vegetables: A review," *Sol. Energy*, vol. 220, pp. 88-110, May 2021, https://doi.org/10.1016/j.solener.2021.03.049

[38] Pratical Action, "Solar Drying." 2007. [Online]. Available: https://infohub.practicalaction.org/bitstreams/533e9cbf-12bf-4c6e-b5ba-e7559738db67/download

[39] E. Getahun, M. Vanierschot, N. Gabbiye, M. A. Delele, S. Workneh, and M. Gebreslasie, "Computational Fluid Dynamic Modeling and Simulation of Red Chili Solar Cabinet Dryer," in *Advances of Science and Technology*, vol. 308, N. G. Habtu, D. W. Ayele, S. W. Fanta, B. T. Admasu, and M. A. Bitew, Eds., in Lecture Notes of the Institute for Computer Sciences, Social Informatics and Telecommunications Engineering, vol. 308., Cham: Springer International Publishing, 2020, pp. 597-609. https://doi.org/10.1007/978-3-030-43690-2_45

[40] Prajapati S, Shah M, Srivastava S. Experimental characterization and thin-layer convective drying modeling of Jamun (Indian Blackberry) slices. Sādhanā 2024; 49: 272. https://doi.org/10.1007/s12046-024-02618-5

[41] Prajapati S, Shah M, Srivastava S. Mass Transfer Behavior of Jamun (Indian Blackberry) Slices Using Convective Drying Technique. J Biosyst Eng 2025; 50: 353-63. https://doi.org/10.1007/s42853-025-00270-3

[42] Prajapati S, Shah M, Srivastava S. Effect of Air Temperature and Velocity on Drying Characteristics of Jamun (Indian Blackberry) Slices Using Convective Drying Method: An Experimental Analysis. In: Kothadia H, Bhardwaj R, Arakeri JH, editors. Proceedings of Fluid Mechanics and Fluid Power (FMFP) 2023, Vol. 4, Singapore: Springer Nature Singapore; 2025, p. 459-67. https://doi.org/10.1007/978-981-97-7388-6_38